Article

Digital colloid-enhanced Raman spectroscopy by single-molecule counting

https://doi.org/10.1038/s41586-024-07218-1

Received: 19 December 2021

Accepted: 21 February 2024

Published online: 17 April 2024

Check for updates

Xinyuan Bi[1], Daniel M. Czajkowsky[1], Zhifeng Shao[1,2] & Jian Ye[1,2,3,4]✉

Quantitative detection of various molecules at very low concentrations in complex mixtures has been the main objective in many fields of science and engineering, from the detection of cancer-causing mutagens and early disease markers to environmental pollutants and bioterror agents[1–5]. Moreover, technologies that can detect these analytes without external labels or modifications are extremely valuable and often preferred[6]. In this regard, surface-enhanced Raman spectroscopy can detect molecular species in complex mixtures on the basis only of their intrinsic and unique vibrational signatures[7]. However, the development of surface-enhanced Raman spectroscopy for this purpose has been challenging so far because of uncontrollable signal heterogeneity and poor reproducibility at low analyte concentrations[8]. Here, as a proof of concept, we show that, using digital (nano)colloid-enhanced Raman spectroscopy, reproducible quantification of a broad range of target molecules at very low concentrations can be routinely achieved with single-molecule counting, limited only by the Poisson noise of the measurement process. As metallic colloidal nanoparticles that enhance these vibrational signatures, including hydroxylamine–reduced-silver colloids, can be fabricated at large scale under routine conditions, we anticipate that digital (nano)colloid-enhanced Raman spectroscopy will become the technology of choice for the reliable and ultrasensitive detection of various analytes, including those of great importance for human health.

The recent implementation of digital quantification in molecular detection strategies, in which analog signals are converted to single-molecule counting, has made notable progress towards the robust and quantitative measurement of very low concentrations of analytes[6,9,10], as particularly shown by digital polymerase chain reaction (dPCR)[1,4,5] and digital enzyme-linked immunosorbent assay (dELISA)[2,3]. However, dPCR is applicable only for detecting pre-targeted DNA and RNA sequences[11], and dELISA is limited by the availability of highly specific antibodies[3], thus restricting their ability to detect nucleic acids and (some) proteins, respectively. In this regard, surface-enhanced Raman spectroscopy (SERS) has long been considered a promising approach because molecular species can be identified without any external identifier, based only on their inherent, unique vibrational signatures[12]. Furthermore, the marked enhancement of signals when the molecule is in electromagnetic hotspots of plasmonic nanostructures has made single-molecule detection possible[13,14]. However, this enhancement cannot be well controlled owing to variable molecular orientations and heterogeneous electromagnetic fields in the hotspots among other factors, leading to notable single-molecule intensity fluctuations (SIFs)[12,15–17]. As a result, quantifications on the basis of integrated intensity of all single-molecule signals (that is, analog measurements) are highly variable at low concentrations, unable to achieve the required reproducibility and accuracy (Extended Data Fig. 1). To mitigate this limitation, efforts have been made to fabricate high-quality solid substrates[17–19]. Yet, until now, these efforts have achieved only modest success with select target molecules[20], unable to meet the challenges of practical applications. Although digitalization of single-molecule SERS signals has been proposed to circumvent this SIFs-induced challenge[21], its implementation with conventional nanostructured solid substrates remains problematic. The main difficulty is that solid substrates are heterogeneous, both in a given substrate and between different substrates, even under strict fabrication conditions (Supplementary Note), and these differences cannot be corrected with calibrations owing to the irreversible nature of the measurement process. Although these variations may not be limiting at high concentrations, reliable and accurate quantifications at low concentrations, even under optimal conditions, cannot be accomplished with confidence[22]. Moreover, the limited number of hotspots in the solid substrates together with the irreversibility of target capture have resulted in few qualified single-molecule events, severely limiting the reliability and sensitivity of the solid-substrate-based approach. In this work, we demonstrate that with metallic colloidal nanoparticles dispersed in aqueous solution, single-molecule Raman signatures of a broad range of molecular targets are sufficiently enhanced to enable the identification of target single molecules, and with single-molecule counting, these target molecules can be reproducibly quantified with unprecedented accuracy, with the Poisson noise of the measurement process ultimately limiting the detection level.

[1]State Key Laboratory of Systems Medicine for Cancer, School of Biomedical Engineering, Shanghai Jiao Tong University, Shanghai, People's Republic of China. [2]National Engineering Research Center of Advanced Magnetic Resonance Technologies for Diagnosis and Therapy, School of Biomedical Engineering, Shanghai Jiao Tong University, Shanghai, People's Republic of China. [3]Institute of Medical Robotics, Shanghai Jiao Tong University, Shanghai, People's Republic of China. [4]Shanghai Key Laboratory of Gynecologic Oncology, Ren Ji Hospital, School of Medicine, Shanghai Jiao Tong University, Shanghai, People's Republic of China. ✉e-mail: yejian78@sjtu.edu.cn

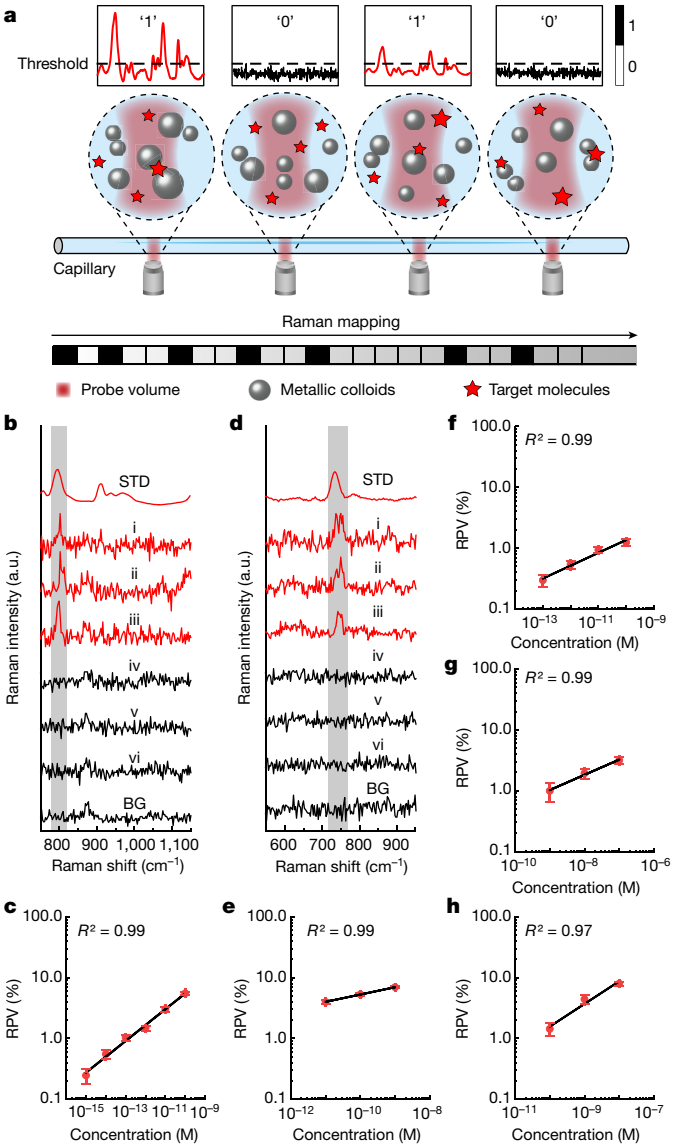

Fig. 1 | The concept of dCERS. a, Schematic of the experiments. The SERS spectra are collected with a quartz capillary containing a suspension of metallic colloidal nanoparticles and target molecules. Each acquisition voxel is assigned as '1' (positive) or '0' (negative) according to whether a single-molecule event is present. **b**, Typical dCERS results obtained with crystal violet. The standard (STD) spectra (top) as well as several examples of single-molecule spectra assigned as positive (i–iii) or negative (iv–vi) are shown. The background (BG) reference spectrum from the null control (bottom) is also shown. The shaded region in these images reflects the signature window for this target molecule. **c**, dCERS calibration curve for crystal violet. **d**, Typical dCERS results for single-stranded DNA (12 nt poly A; A12). The spectra shown are as described in **b**. **e**, dCERS calibration curve for A12. **f**–**h**, The dCERS curves for 4-nitrobenzenethiol (4-NBT) (**f**), D-glucose (**g**) and haemoglobin (**h**) are also shown. RPV, ratio of positive voxels. Error bars were calculated from three independent measurements. Hya–Ag colloidal nanoparticles (about 24 nm in diameter) at 0.5 nM were used for all these measurements. a.u., arbitrary units.

In our system, we used a quartz capillary (inner diameter 1 mm) containing 10 µl of a metallic colloid suspension to generate enhanced Raman spectra from target molecules (Fig. 1a and Extended Data Fig. 2). A scanning probe system (0.3 numerical aperture, 10× objective lens, 638 nm excitation wavelength) was used to acquire the Raman spectra from each sample in a pointwise scanning mode. Silver colloids (20–50 nm in diameter) were used for their dispersion stability during measurements and their excellent Raman enhancement abilities[7]. The most effective colloidal concentration for these measurements was experimentally determined (Methods) owing to the fact that while the number of hotspots increases with the concentration of the colloids, the background scattering also increases at the same time, leading to a reduction of detectable signals. In contrast to solid substrates, the monodispersed silver colloids exhibit homogeneous distributions throughout the entire suspension, ensuring a nearly uniform probability of the colloid–target interactions throughout the data acquisition chamber (Extended Data Fig. 3). To satisfy the criterion of independence for sequentially acquired measurements, the acquisition is performed with neighbouring voxels spaced sufficiently far apart (here, 10 µm) to minimize the possibility of double sampling (Methods). For digitization, each voxel is designated as positive ('1') if the signal of the specific vibrational signature is above a preset threshold that is determined by the fluctuations in the noise window, and as negative ('0') otherwise.

With this system, we first verified its single-molecule sensitivity and the appropriate range for single-molecule counting with the bi-analyte SERS technique (Methods and Extended Data Fig. 4) using hydroxylamine-reduced silver (Hya–Ag) colloids (ζ potential: −35.6 mV) at 0.5 nM, which was found to be optimal (Extended Data Fig. 3). Hya–Ag colloids at this concentration remained monodispersed in suspension over time, ensuring a statistically uniform distribution of hotspots throughout the measurement in space and time (Methods and Extended Data Fig. 3). The acquisition time was chosen as 0.1 s or 1 s for different target molecules depending on their signal strength to balance the signal-to-noise ratio (thus the reliability of single-molecule identification) and detection efficiency (the number of qualified single-molecule events in a given period). We used the maximum intensity (I_s) in the spectral window containing the specific signature for the measured molecule after baseline removal to identify the target molecules. We note that the appropriate concentration range for single-molecule counting is expected to vary over a broad range, owing to the complex nature of the target–hotspot interactions. As shown in Extended Data Fig. 4, for crystal violet molecules, single-molecule events were found to be dominant below 10^{-9} M, but for 4-nitrobenzenethiol (4-NBT), a concentration below 10^{-8} M was necessary. Therefore, the appropriate single-molecule range for an intended target molecule must be pre-determined to satisfy the requirements of digital (nano)colloid-enhanced Raman spectroscopy (dCERS).

To demonstrate the concept of dCERS, we examined several representative target molecules at various concentrations following the procedure described above. An example of crystal violet is shown in Fig. 1b and Extended Data Fig. 5a, in which the signature window was from 780 cm^{-1} to 820 cm^{-1} (out-of-plane C–H bending[23]) in which unique peaks were present. To assign '1' or '0' to each voxel, I_s was compared with a preset threshold, which was experimentally determined by calculating the mean ($\bar{x}$) and the standard deviation (σ) in a window away from the signature window in which no apparent peaks are present. In the case of crystal violet, we used a window from 1,700 cm^{-1} to 1,740 cm^{-1} in the same spectrum and chose $I_s - \bar{x} \geq 10\sigma$ as the threshold. The reason for choosing this relatively high threshold is to achieve a low false-positive rate (less than two over 5,400 voxels with null controls in this case) at the cost of a lower detection efficiency. However, the most appropriate threshold should be determined as a balance between the desired accuracy (the number of positive counts, see below) and a reasonable acquisition time (see below and Methods). It should also be noted that for any analyte to be suitable for dCERS detection, well-recognized spectral features must be present without marked complications either from the background or from other analyte species and adequate analyte–colloid interaction should be ensured by a suitable colloidal surface functionalization (Methods).

Using the above criteria, the ratio of positive voxels to the total number of measured voxels (RPV) was found to change monotonically with the crystal violet concentration, as expected (Extended Data Fig. 6a).

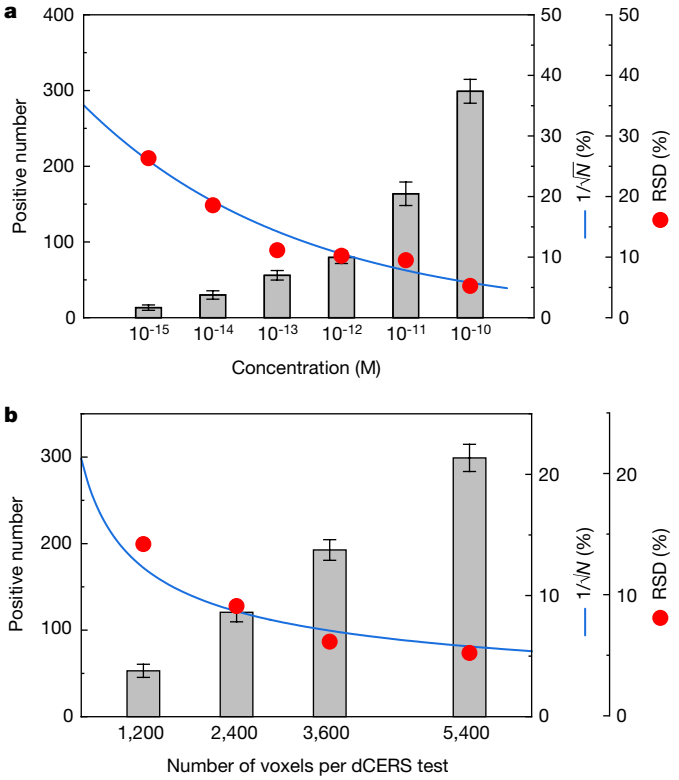

Fig. 2 | Reproducibility of dCERS. a, The dependency of the mean number of positive counts (grey bars) on the concentration of crystal violet under a fixed number of measured voxels per dCERS test (5,400 voxels). The error bars indicate the standard deviations ($n = 3$). The RSDs (red dots) and the expectation based on Poisson statistics (blue curve) are also shown. **b**, Dependency of the mean number of positive voxels on the voxel number at 10^{-10} M crystal violet ($n = 3$). The RSD and expectation based on Poisson statistics as in **a** are also shown.

The concentration dependence of RPV for crystal violet is well described by a straight line with $R^2 = 0.99$ when plotted on a log–log scale (Fig. 1c), as expected for adsorption events at low analyte concentrations on the basis of classical Gibbs thermodynamics[24,25]. We note that this relationship is not unique for crystal violet, as all other target molecules studied here, from the relatively simple glucose to poly-nucleic acids and proteins, exhibit the same linear relationship on the log–log plot (Fig. 1d–h and Extended Data Fig. 6). In practical applications, the highly reproducible nature of these monotonic correspondences between the analyte concentration and the single-molecule events should be sufficiently adequate to convert the measured RPVs to the actual concentrations, provided a pre-calibration is conducted for each analyte and/or each batch of fabricated colloids (see Methods, Extended Data Table 1 and Extended Data Fig. 6).

We next sought to quantify the accuracy of these measurements, an equally important aspect for reliable quantifications of target analytes. As single-molecule-based measurements are essentially an accumulation of discrete single-molecule events, a reasonable assumption is that these measurements should follow a Poisson distribution[26], regardless of the details of the measurement process. As such, the measurement error should be simply the square root of the total counts of the single-molecule events per measurement at each concentration[21]. We thus made multiple measurements at several concentrations and calculated the mean and the measurement error at each concentration, using crystal violet and Hya–Ag colloids as a test case. As shown in Fig. 2a, the relative standard deviation (RSD) of the measured single-molecule events for each concentration is consistent with a Poisson distribution and varies as $1/\sqrt{N}$, where N is the total number of positive single-molecule events with 5,400 total voxels per measurement (Fig. 1c). Therefore, it immediately follows that the accuracy of a single measurement for a particular concentration must improve as more positive voxels are measured, which would require more voxels to be acquired, and thus a longer measurement period. As demonstrated in Fig. 2b, for the case of crystal violet at 10^{-10} M, the RSD ($n = 3$) was reduced from 14.2% to 5.3% when the accumulated positive voxels increased from 53 to 299 with an increase in the total number of acquired voxels from 1,200 to 5,400, precisely as predicted by the square-root law. This result was further verified at other concentrations (Extended Data Fig. 7a) as well as for several different analyte molecules in the single-molecule regime (Extended Data Fig. 7b). These results strongly indicate that measurements on the basis of discrete single-molecule events should largely follow a Poisson distribution in general and, as such, the achievable measurement accuracy should be determined (and predicted) by the accumulated positive events, which is solely limited by the acceptable measurement duration and the number of false positives (of the background) in the measurement period regardless of the analyte concentration or the detection efficiency of a particular system. When the RPV and its uncertainty are known, the actual analyte concentration along with its accuracy can then be recovered from the pre-calibrated correspondence curve.

To further demonstrate the validity of dCERS, we quantified a mixture of two different target molecules dispersed in the same solution, crystal violet and Nile blue, at various concentrations (Methods). To digitize the single-molecule signal of Nile blue in each voxel, we used I_s in the window from 565 cm^{-1} to 605 cm^{-1} corresponding to its characteristic peak at 585 cm^{-1} (Extended Data Fig. 5b), which does not overlap with that of crystal violet (800 cm^{-1}) or the background peaks present in the null control (Extended Data Fig. 5a). The calibration between RPV and the Nile blue concentration is shown in Extended Data Fig. 6k, again showing a linear relationship on the log–log scale. Figure 3a shows the typical single-molecule spectra of crystal violet and Nile blue when both are present in the sample. It is noted that in these traces, the signal present in a particular voxel was generated either by crystal violet or by Nile blue but very rarely both at these concentrations, consistent with the expectation that at very low concentrations, single-molecule events dominate. Figure 3b shows the measured results for these mixed samples at various concentrations of crystal violet and Nile blue (Methods), each showing the same relationship as that measured when only one analyte is present. Furthermore, the concentrations of both crystal violet and Nile blue were also accurately determined despite the two orders of magnitude difference in terms of the relative concentrations of the two analytes (that is, 10^{-11} M for crystal violet and 10^{-13} M for Nile blue). The standard deviations calculated from triplicate measurements at each mixture were also consistent with Poisson statistics. These results demonstrate that dCERS can achieve simultaneous quantification of multiple target analytes solely on the basis of their characteristic SERS signatures over broad concentration ranges, provided that the analyte concentrations satisfy the single-molecule requirement, namely, that they are sufficiently low.

We further tested the detection capabilities of dCERS by examining minute amounts of paraquat in solution, a highly toxic herbicide that could cause Parkinson's disease[27] and has been banned in 32 countries[28]. We calibrated paraquat at concentrations from 10^{-8} M to 10^{-10} M in pure water with the same Hya–Ag colloids using 1,620–1,660 cm^{-1} as the signature window. It is not insignificant to note that with only 2,400 voxels acquired for each measurement, we achieved an RSD of 11% at a paraquat concentration of 10^{-10} M ($n = 3$) (Extended Data Fig. 6l), which is three orders of magnitude lower than the maximum residual level of paraquat established by the European Union[29]. In comparison, current technologies, such as UV spectrophotometry[30], can detect only paraquat at concentrations in the 2×10^{-7} M range. To further determine whether such measurements could also be achieved under complex and uncharacterized backgrounds similar to field situations, we then

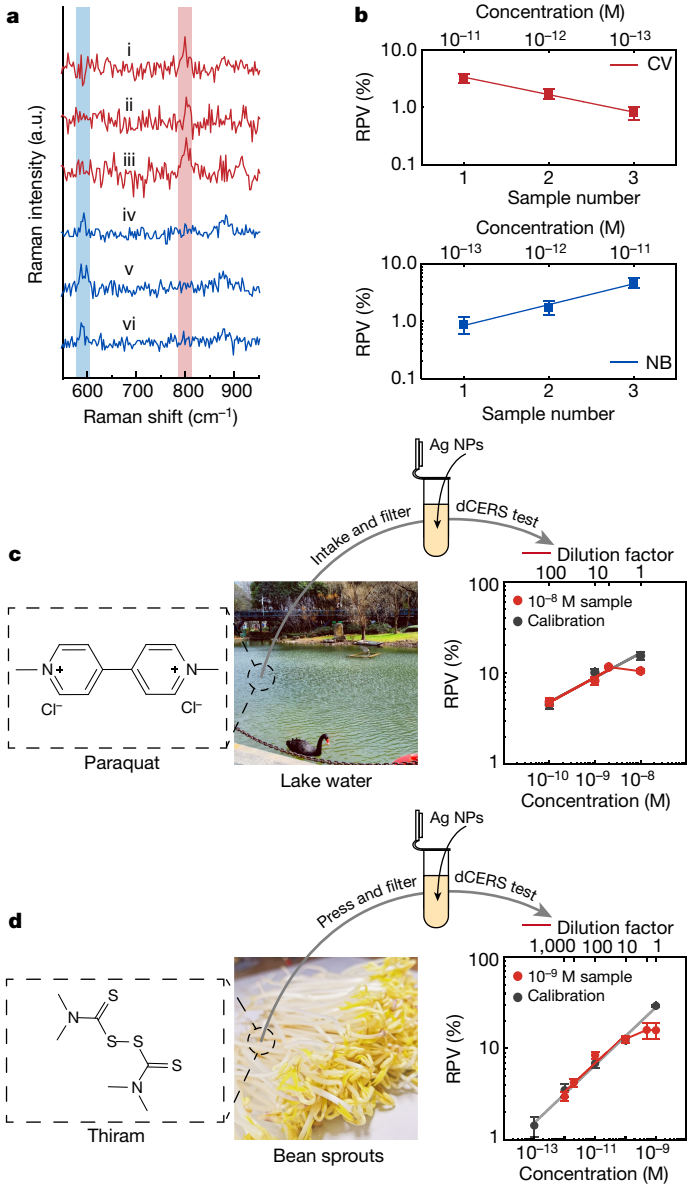

Fig. 3 | Quantitative detection of trace amount of chemicals by dCERS. **a**,**b**, Quantification of crystal violet and Nile blue when mixed at three different concentration proportions (denoted by sample numbers 1, 2 and 3). Typical single-molecule spectra (**a**) corresponding to crystal violet (i–iii) (red, '0' for Nile blue and '1' for crystal violet) and Nile blue (iv–vi) (blue, '1' for Nile blue and '0' for crystal violet) in a mixed sample. The characteristic peaks (shaded with corresponding colour) for crystal violet and Nile blue are identified and used for quantification. RPV versus the concentrations of crystal violet (CV) (top) and Nile blue (NB) (bottom) in the three samples (**b**), fitted by a linear equation on the log–log scale. The total acquisition voxels were 1,200 for each measurement. **c**, When the highly toxic herbicide paraquat was added to normal lake water, 10^{-8} M (red dots) paraquat were readily detected with 5-fold, 10-fold and 100-fold dilution. However, there was notable competition at the original concentration, and the same linear relationship was recovered only on sufficient dilution (compared with calibration denoted by black dots). Inset, chemical structure of paraquat. **d**, With fungicide thiram dissolved in the bean sprouts extract (10^{-9} M), dCERS was also effective even when diluted by a 1,000-fold. However, similar to the case with lake water, the competition owing to the residual materials was significant at the original concentration. But accurate measurement was achieved on further dilution. Inset, chemical structure of thiram. All the error bars indicate the standard deviations ($n = 3$). NP, nanoparticle.

tested paraquat dissolved in lake water. We first passed the lake water drawn from a local pond through membrane filters of different cut-offs (see Methods for details) to remove particulates and aggregates to reduce background scattering. After confirming that the filtered lake water exhibited characteristics in the range for normal lake water established by the US Environmental Protection Agency[31] (Methods), paraquat was added to the filtered lake water to a concentration of 10^{-8} M. We then performed dCERS measurements with a series of dilutions, and the results are shown in Fig. 3c. It is noted that at 10^{-8} M (without dilution), the measured RPV was substantially lower than that predicted by the calibration curve, indicating that the competition from the residual materials present in the filtered laker water was significant. However, on dilution, the same log–log linear correspondence as that obtained in the calibration was achieved, and the paraquat concentration was accurately determined after multiplication by the dilution factor. Therefore, for samples with a complex and unknown background, sufficiently low concentrations are necessary to mitigate potential competitions for the hotspots to achieve reliable quantification of the target molecules. Hence, serial measurements over a broad dilution range may be necessary, and only when the calibrated linear correspondence is achieved can there be confidence about the determined concentration. It is noted that even at 10^{-10} M (after 100-fold dilution), the paraquat concentration was still accurately determined (1.04×10^{-10} M) with a total of 2,400 voxels acquired (40 min), which could be further improved if additional voxels were acquired.

As a final proof of its validity, we applied dCERS to the detection of a fungicide, thiram, that is highly toxic[32] and has been classified as a carcinogen category 2 toxicant by the European Union[33,34]. More recently, the European Union has advised against the use of thiram for any agricultural purposes[35]. We first established the calibration curve of thiram in pure water from 10^{-9} M to 10^{-13} M with the Hya–Ag colloids using 1,360 cm^{-1} to 1,400 cm^{-1} as the signature window (Extended Data Fig. 6m). Because our main objective is to measure the residual thiram in agricultural products, we used extracts from laboratory-grown bean sprouts as a model system (Methods and Extended Data Fig. 8). The sprouts were homogenized, centrifuged and membrane-filtered to produce the extracts (Methods). Thiram was then dissolved in the extract at a concentration of 10^{-9} M (equivalent to 2.4×10^{-4} mg kg^{-1}). Similar to paraquat, measurements of a serial dilution were performed, and the results are shown in Fig. 3d. Once again, significantly lower values were found at the original concentration (10^{-9} M), most likely also owing to the competition of the materials retained in the extract. But on further dilution, the same linear relationship as the calibration was recovered at concentrations below 10^{-10} M. Even at 10^{-13} M, which is about five orders of magnitude lower than the detection limit of liquid chromatography-tandem mass spectrometry[33], dCERS measurements are robust and reliable, achieving an error of 25% with only 2,400 total voxels acquired. These two examples demonstrate the unparalleled advantage of dCERS in detecting very low concentrations of soluble target molecules at accuracies that can be directly estimated on the basis of accumulated positive counts. Moreover, these experiments also indicate that measurements with serial dilutions are required to sufficiently reduce any influence from unknown background components to enable correspondence with the calibrations. As such, this procedure requires the colloidal system to be consistent and reproducible, which is a substantial challenge with solid chip-based systems.

In conclusion, we have demonstrated that dCERS based on single-molecule counting is an effective and efficient technology for molecular quantifications at ultralow concentrations solely on the basis of intrinsic vibrational signatures of the target molecules as long as they exhibit well-defined, specific spectral signatures as well as adequate interaction with the hotspots. As demonstrated by the proof-of-concept examples with the toxic compounds (thiram and paraquat), the unprecedented sensitivity and predictable accuracy make dCERS a powerful and perhaps even preferred technology for

demanding applications, including environmental protection, food safety and mutagen detection, in which the presence of even a trace amount of certain chemicals could already be a serious threat to human health.

Online content

Any methods, additional references, Nature Portfolio reporting summaries, source data, extended data, supplementary information, acknowledgements, peer review information; details of author contributions and competing interests; and statements of data and code availability are available at https://doi.org/10.1038/s41586-024-07218-1.

1. Vogelstein, B. & Kinzler, K. W. Digital PCR. *Proc. Natl Acad. Sci. USA* **96**, 9236–9241 (1999).
2. Rissin, D. M. & Walt, D. R. Digital concentration readout of single enzyme molecules using femtoliter arrays and Poisson statistics. *Nano Lett.* **6**, 520–523 (2006).
3. Rissin, D. M. et al. Single-molecule enzyme-linked immunosorbent assay detects serum proteins at subfemtomolar concentrations. *Nat. Biotechnol.* **28**, 595–599 (2010).
4. Hindson, C. M. et al. Absolute quantification by droplet digital PCR versus analog real-time PCR. *Nat. Methods* **10**, 1003–1005 (2013).
5. Heyries, K. A. et al. Megapixel digital PCR. *Nat. Methods* **8**, 649–651 (2011).
6. Giljohann, D. A. & Mirkin, C. A. Drivers of biodiagnostic development. *Nature* **462**, 461–464 (2009).
7. Lane, L. A., Qian, X. & Nie, S. SERS nanoparticles in medicine: from label-free detection to spectroscopic tagging. *Chem. Rev.* **115**, 10489–10529 (2015).
8. Wang, X., Huang, S.-C., Hu, S., Yan, S. & Ren, B. Fundamental understanding and applications of plasmon-enhanced Raman spectroscopy. *Nat. Rev. Phys.* **2**, 253–271 (2020).
9. Salk, J. J., Schmitt, M. W. & Loeb, L. A. Enhancing the accuracy of next-generation sequencing for detecting rare and subclonal mutations. *Nat. Rev. Genet.* **19**, 269–285 (2018).
10. Liu, H. & Lei, Y. A critical review: recent advances in "digital" biomolecule detection with single copy sensitivity. *Biosens. Bioelectron.* **177**, 112901 (2021).
11. Baker, M. Digital PCR hits its stride. *Nat. Methods* **9**, 541–544 (2012).
12. Qian, X.-M. & Nie, S. M. Single-molecule and single-nanoparticle SERS: from fundamental mechanisms to biomedical applications. *Chem. Soc. Rev.* **37**, 912–920 (2008).
13. Nie, S. & Emory, S. R. Probing single molecules and single nanoparticles by surface-enhanced Raman scattering. *Science* **275**, 1102–1106 (1997).
14. Kneipp, K. et al. Single molecule detection using surface-enhanced Raman scattering (SERS). *Phys. Rev. Lett.* **78**, 1667–1670 (1997).
15. Zong, C. et al. Single-molecule level rare events revealed by dynamic surface-enhanced Raman spectroscopy. *Anal. Chem.* **92**, 15806–15810 (2020).
16. Etchegoin, P. G. & Le, Ru,E. A perspective on single molecule SERS: current status and future challenges. *Phys. Chem. Chem. Phys.* **10**, 6079–6089 (2008).
17. Bell, S. E. J. et al. Towards reliable and quantitative surface-enhanced Raman scattering (SERS): from key parameters to good analytical practice. *Angew. Chem. Int. Ed.* **59**, 5454–5462 (2020).
18. Yao, X. et al. Uniform periodic bowtie SERS substrate with narrow nanogaps obtained by monitored pulsed electrodeposition. *ACS Appl. Mater. Interfaces* **12**, 36505–36512 (2020).
19. Cong, S. et al. Electrochromic semiconductors as colorimetric SERS substrates with high reproducibility and renewability. *Nat. Commun.* **10**, 678 (2019).
20. Bhavya, M. B. et al. Femtomolar detection of thiram *via* SERS using silver nanocubes as an efficient substrate. *Environ. Sci. Nano* **7**, 3999–4009 (2020).
21. de Albuquerque, C. D. L., Sobral-Filho, R. G., Poppi, R. J. & Brolo, A. G. Digital protocol for chemical analysis at ultralow concentrations by surface-enhanced Raman scattering. *Anal. Chem.* **90**, 1248–1254 (2018).
22. Fan, M., Andrade, G. F. & Brolo, A. G. A review on recent advances in the applications of surface-enhanced Raman scattering in analytical chemistry. *Anal. Chim. Acta* **1097**, 1–29 (2020).
23. Harraz, F. A. et al. Surface-enhanced Raman scattering (SERS)-active substrates from silver plated-porous silicon for detection of crystal violet. *Appl. Surf. Sci.* **331**, 241–247 (2015).
24. Lu, L. & Na, C. Gibbsian interpretation of Langmuir, Freundlich and Temkin isotherms for adsorption in solution. *Philos. Mag. Lett.* **102**, 239–253 (2022).
25. Na, C. Size-controlled capacity and isocapacity concentration in Freundlich adsorption. *ACS Omega* **5**, 13130–13135 (2020).
26. Gallager, R. G. in *Discrete Stochastic Processes* 31–55 (Springer, 1996).
27. Gawarammana, I. B. & Buckley, N. A. Medical management of paraquat ingestion. *Br. J. Clin. Pharmacol.* **72**, 745–757 (2011).
28. Dorsey, E., Sherer, T., Okun, M. S. & Bloem, B. R. The emerging evidence of the Parkinson pandemic. *J. Parkinsons Dis.* **8**, S3–S8 (2018).
29. Commission Regulation (EU) No 520/2011 of 25 May 2011 amending Annexes II and III to Regulation (EC) No 396/2005 of the European Parliament and of the Council as regards maximum residue levels for benalaxyl, boscalid, buprofezin, carbofuran, carbosulfan, cypermethrin, fluopicolide, hexythiazox, indoxacarb, metaflumizone, methoxyfenozide, paraquat, prochloraz, spirodiclofen, prothioconazole and zoxamide in or on certain products. *Official Journal of the European Union* (2011); https://eur-lex.europa.eu/LexUriServ/LexUriServ.do?uri=OJ:L:2011:140:0002:0047:EN:PDF.
30. de Almeida, R. M. & Yonamine, M. Enzymatic-spectrophotometric determination of paraquat in urine samples: a method based on its toxic mechanism. *Toxicol. Mech. Methods* **20**, 424–427 (2010).
31. United States Environmental Protection Agency. *5.9 Conductivity*, https://archive.epa.gov/water/archive/web/html/vms59.html (2023).
32. EFSA& Dujardin, B. Comparison of cumulative dietary exposure to pesticide residues for the reference periods 2014–2016 and 2016–2018. *EFSA J.* **19**, e06394 (2021).
33. European Food Safety Authority. Peer review of the pesticide risk assessment of the active substance thiram. *EFSA J.* **15**, e04700 (2017).
34. Regulation (EC) No 1272/2008 of the European Parliament and of the Council of 16 December 2008 on classification, labelling and packaging of substances and mixtures, amending and repealing Directives 67/548/EEC and 1999/45/EC, and amending Regulation (EC) No 1907/2006. *Official Journal of the European Union* **353**, 1–1355 (2008).
35. Commission Implementing Regulation (EU) 2018/1500 of 9 October 2018 concerning the non-renewal of approval of the active substance thiram, and prohibiting the use and sale of seeds treated with plant protection products containing thiram, in accordance with Regulation (EC) No 1107/2009 of the European Parliament and of the Council concerning the placing of plant protection products on the market, and amending Commission Implementing Regulation (EU) No 540/2011. *Official Journal of the European Union* **254**, 1–3 (2018).

Methods

Materials and instrumentation

Chloroauric chloride ($HAuCl_4 \cdot 4H_2O$) and ethanol (≥99.7%) were purchased from Sinopharm Chemical Reagent. Silver nitrate ($AgNO_3$, 99.8%), sodium citrate (98%), hydroxylammonium chloride (Hya · HCl, 99%), potassium chloride (KCl, 99.5%) and sodium hydroxide (NaOH, ≥98%) were all purchased from Aladdin. D-Glucose (≥99.5%), L-cysteine (≥98.5%), thiram (97%) and human haemoglobin were purchased from Sigma-Aldrich. 4-Nitrobenzenethiol (4-NBT, 90%), Nile blue, crystal violet (95%) and paraquat (99.7%) were purchased from Fluorochem, Alfa Aesar, Absin and Macklin, respectively. Single-stranded DNA, A12 (sequence from 5′ to 3′: AAA AAA AAA AAA), was synthesized by Sangon Biotech. Nanopure water (18.2 MΩ) was used for all experiments. All materials were used without further purification.

The morphology of colloids was characterized by a JEM-2100F transmission electron microscope (JEOL). A UV1900 UV–Vis spectrophotometer (Aucybest) was used to obtain the extinction spectra of the colloidal suspensions. The concentrations of the colloidal suspensions were measured by a nanoparticle tracking analyser (ZetaView). The hydrodynamic diameter (Extended Data Fig. 3) and the ζ potential of the SERS colloids as well as the particulate content of the lake water were characterized by a Zetasizer Nano ZSP (Malvern). The ζ potential of the Hya–Ag colloids, citrate–Ag colloids and citrate–Au colloids were −35.6 mV, −33.8 mV and −36.0 mV, respectively. The conductivity and the pH of the lake water were measured to be 154.4 μS cm^{-1} and 7.9 by a SevenCompact S230 Conductivity Meter (METTLER TOLEDO) and a SevenCompact S220 pH/Ion Meter (METTLER TOLEDO), respectively, and without measurable changes after the addition of paraquat.

Fabrication and characterization of SERS colloids

For Hya–Ag colloids, 1 ml $AgNO_3$ (10 mM) was added quickly into a 9-ml mixture of Hya · HCl (1.67 mM) and NaOH (3.33 mM) and then stirred vigorously, according to the optimized protocol in ref. 36. Citrate–Ag colloids and citrate–Au colloids were both prepared following the methods in ref. 37. In detail, to synthesize citrate–Ag colloids, $AgNO_3$ solution (18 mg in 100 ml H_2O) was heated to boil and then 2 ml of a sodium citrate solution (1%) was added dropwise for 2 min, followed by 1-h boiling to obtain the final colour of a greenish yellow. For citrate–Au colloids, an $HAuCl_4$ solution (48 mg in 100 ml H_2O) was brought to boil and then mixed with 10 ml of a sodium citrate solution (1%). The colour of the mixture was found to change from light yellow to dark blue and then to wine red after about 15 min of boiling. The mixture was boiled for another 30 min, followed by the immersion of the flask containing the products into ice-cold water to quench the reaction[38].

For dCERS, the detection efficiency is closely related to the colloidal concentration as a result of the hotspot density in the voxels and the colloidal background scattering, which should, therefore, be optimized to balance the two factors. The former refers to the areas adjacent to the colloidal surface with a high electromagnetic field, in which the SERS signals of the molecules can be greatly enhanced and has the potential to generate positive voxels if in the probe volume. Therefore, the colloidal concentration is desired to be higher to increase the hotspot density, making the molecules more likely to be detected. The second issue is the background scattering, which, on the contrary, is preferred to be low. Too many colloids scatter the molecular SERS signals, thus reducing the usable hotspots. We examined this issue using Hya–Ag colloids (from 0.17 nM to 1.5 nM) with 10^{-10} M crystal violet and 10^{-7} M L-cysteine as examples. With both samples, the optimal concentration of Hya–Ag colloids was found to be 0.5 nM (Extended Data Fig. 3k,l). Although the precise optimal colloidal concentration is likely to vary among different analytes, the optimal range was found to be relatively broad. Therefore, a reasonable choice of colloidal concentrations (for example, 0.5 nM) should be generally adequate for most measurements. Achieving the same accuracy at suboptimal concentrations would require only an increase in the measurement time, which is a strong advantage of this method. Experiments with other colloids were also adjusted to 0.5 nM on the basis of nanoparticle tracking analyser counts.

SERS colloid–molecule suspension preparation

L-Glucose, D-cysteine, paraquat, thiram, haemoglobin and A12 were dissolved in H_2O at the desired concentrations, and 4-NBT, crystal violet and Nile blue were dissolved in ethanol. They were mixed with SERS colloids in a ratio of 1:9. Immediately after mixing, all samples were ultrasonicated for about 20 s for mixing consistency and incubated for 1 h at room temperature. Immediately before measurements, the stored samples were slightly ultrasonicated for about 3 s to prevent the precipitation of the colloids. For the quantification of crystal violet and Nile blue mixed in solution, three samples were prepared with different concentration proportions—namely, 10^{-13} M, 10^{-12} M and 10^{-11} M for Nile blue and 10^{-11} M, 10^{-12} M and 10^{-13} M for crystal violet for samples 1, 2 and 3, respectively. For quantification of paraquat and thiram, the lake water was collected from Xujiahui Park in Shanghai, China. The bean sprouts were grown in the laboratory and harvested after a 6-day culture under normal growth conditions. After washing with pure water, the bean sprouts were pressed into juice (10 g bean sprouts in 10 ml ultrapure water) to obtain a homogenized sample. Following centrifugation, the samples were filtered using membranes with 0.8 μm, 0.22 μm and 3 kDa cutoff to prepare the extract. Paraquat and thiram at the desired concentrations were added into the above pretreated lake water and bean sprout extract, respectively.

SERS data acquisition

The mixture of colloids and molecules (10 μl) was injected into a quartz capillary (outer diameter 2 mm, inner diameter 1 mm). SERS data acquisition was performed with a confocal Raman system (Horiba, XploRA INV) along the longitudinal axis (one dimension) of the capillary in the point-by-point scanning mode with a step size of 10 μm. For concentrations requiring more voxels, spectra were acquired in the two-dimensional mode. SERS spectra were collected using a 10× objective lens (numerical aperture 0.3). Other measurement parameters are indicated in Extended Data Table 2.

Validation of the Bernoulli trial

In this method, each voxel is considered to be a Bernoulli trial—that is, a yes-or-no question with a probability p for '1' (positive) and a probability $q = 1 - p$ for '0' (negative). Then the summed binarized value of all voxels in a sample is expected to follow a Poisson distribution (a limiting case of the Bernoulli distribution). For this, it is required that the voxels are identically distributed and independent random variables. To show uniformity among voxels, we examined the signal variation among voxels at a relatively high concentration of analyte, and this was found to be very low (Extended Data Fig. 3j). We note that identical imaging parameters are used throughout this measurement, ensuring a constant excitation volume, and that these Hya–Ag SERS colloids remain well dispersed during the experiment, with dynamic light scattering showing a highly stable suspension without obvious aggregation even after 3 h of measurement (the maximal duration used in the work) (0 min: 39.9 ± 16.3 nm, polydispersity index (PDI) = 0.323; 1 h: 40.1 ± 15.8 nm, PDI = 0.272; 3 h: 41.3 ± 17.9 nm, PDI = 0.228) or even longer and after the addition of different analytes (10^{-10} M crystal violet: 39.2 ± 15.9 nm, PDI = 0.321; 10^{-8} M paraquat: 43.9 ± 21.2 nm, PDI = 0.274; 10^{-9} M thiram: 44.2 ± 21.2 nm, PDI = 0.344). To ensure the independence of separate measurements, the step size should be larger than the excitation volume so that the neighbouring voxels do not overlap and are sufficiently spaced apart. Given that the diameter of the excitation volume with the 10× objective lens is 2.69 μm (= 1.22 × 0.638 μm/0.3), a step size of 10 μm guaranteed that there was no double sampling.

Determination of positive voxels

All SERS spectra were baseline-corrected with the Horiba LabSpec software. The maximum intensity (I_s) in a window containing the characteristic Raman peaks of the target molecule was used to determine whether a molecule was detected in that voxel. For digitalization, the voxel is assigned positive ('1') when I_s was greater than the threshold calculated from a 'background' window or negative ('0') otherwise. We note that the signature window should be chosen at a unique band of the target molecule as well as away from other peaks present in the null control, whereas the noise region should be selected away from any peaks belonging to the target molecule and the null control. When choosing a proper threshold, factors such as confidence level in determining a positive peak at certain spectra and false positives in the null controls (that is, the background sample without target analytes) under the same measurement parameters should be taken into consideration. To determine the threshold in our experiment, we expected that the intensity follows a normal distribution if most signals are just noise ($X \sim N(\mu, \sigma^2)$). The set of the intensities in the signature window is a sample therefrom and the peak intensity is the maxima from the sample (X_n).

$$F(X_n > x) = 1 - F(X_n \le x) = 1 - \prod_{i=1}^{n} F(X_i \le x) = 1 - (F(x))^n$$

For example, with crystal violet, the signature window was from 780 cm^{-1} to 820 cm^{-1} with 16 intensity numbers ($n = 16$) and 5,400 voxels were collected in each dCERS test. We set the probability of false positives to be less than ((1/5,400) × 100%), theoretically. Then,

$$F(X_n > x) = 1 - (F(x))^{16} < \frac{1}{5{,}400}$$

$$F(\mu + 5\sigma) > F(x) \approx 0.999988425 > F(\mu + 4\sigma)$$

Furthermore, we found $\mu \approx \mu_{noise}$, $\sigma \approx 2\sigma_{noise}$ (noise window at 1,700–1,740 cm^{-1} with no apparent peak present; Extended Data Fig. 5). So, when the noise window was used to estimate the signature window, the threshold was determined to be ($\mu_{noise} + 10\sigma_{noise}$). When a measurement process is Poisson-dominated, the actual limit of detection (LOD) is determined only by the null control[39] (that is, the false positives over the measuring period). As long as the positive number counted from an unknown sample is higher than the false positives in the null control with confidence, this sample can be quantified under the current conditions. Therefore, the false positives are preferred to be extremely low so that the lowest possible concentration can still be successfully quantified provided that enough positive detection events have been accumulated for an intended accuracy. For instance, the null control for the detection system of crystal violet was measured to be only two false positives in the null control when 5,400 voxels were acquired in total (RPV ≈ 0.037%). Thus, the theoretical LOD is estimated to be 3.6×10^{-17} M with the false positives and three times the error based on the calibration curve, indicating that we should be able to quantify concentrations even much lower than the 1 fM (RPV ≈ 0.25%) demonstrated in the main text. In practice, methods such as spectral fitting might further reduce the false positives in the null control and improve the confidence of positive judgement (though not provided in this work), thus improving the LOD of the dCERS. A higher threshold can also be used yet at the cost of reducing single-molecule events at a certain analyte concentration, whereas a lower threshold may include more false positives thus reducing the accuracy as well as increasing the lower bound of the detection limit (that is, 250 false positives in 5,400 voxels at 5σ threshold and even 1,689 in 5,400 at 3σ threshold). Details about the choice of signature windows, background windows and thresholds for all targeted molecules discussed in this work are found in Extended Data Table 2.

Single-molecule sensitivity using the bi-analyte SERS technique

To determine the single-molecule sensitivity of the SERS colloids and the concentration range for dCERS that is not necessary in analog quantification, we used the bi-analyte SERS (BiASERS) technique, a widely accepted method to examine the single-molecule sensitivity of SERS colloids and to determine a genuine single-molecule event[40]. In short, two types of analyte were mixed together and incubated with the colloids. Here, we used crystal violet and Nile blue and 4-NBT/4-Chlorothiophenol (4-CBT) as two groups of bi-analytes, because in each group, the analytes had similar cross-sections and resonances under the excitation laser wavelength (that is, 638 nm). In this assay, the concentrations of the two analytes are not necessarily the same, being adjusted to obtain comparable numbers of pure events in one mixture (see the legend of Extended Data Fig. 4) because of their unavoidable differences in their affinity to the NPs and the other factors. When both analytes were at relatively higher concentrations, the spectra collected were dominated by mixed signals, as each spectra showed signals of both analytes, whereas only a minority or none of the spectra showed the pure signals (having the signals of only one of the analytes). As the concentrations of both analytes were simultaneously lowered, there could be only a couple of mixed signals or even a single or no signals captured in each acquisition, gradually leading to the dominance of pure events in the spectral set. Statistically, the pure events were most likely to be generated by a single molecule. Therefore, at this concentration and below, the acquired pure events should be dominated by single-molecule events. At the same time, if a large number of pure events can be obtained by the SERS colloids, we recognized this type of colloids to be single-molecule sensitive with abundant single-molecule-sensitive hotspots. With further decreases in the concentration of the analyte molecules, there would be a decrease in the proportion of signal spectra and an increase in the proportion of single-molecule events for the single-molecule-sensitive SERS colloids. These expectations were borne out by the experiments (Extended Data Fig. 4).

Calibration curve for dCERS

For dCERS, the RPV is directly calculated as the ratio of positive voxels to the acquired total voxels. On the basis of classical Gibbs thermodynamics for adsorption binding events at very low concentrations in solution, we expected that the relationship between RPV and concentration should be linear on a log–log scale, as typically described by the Freundlich equation[41]. Therefore, the data obtained with pure analytes in water were fitted to a linear curve in the log–log plot to obtain the calibration curve ($\log RPV = k \log M + b$). For higher concentrations beyond this calibrated range, dilution of the sample may be necessary to make the concentration fall into this range.

dCERS quantification accuracy

As the quantification of each concentration is simply a counting process of single-molecule binding events, the number of detectable analyte–colloid interactions (N) determines the ratio of positive voxels according to the Poisson distribution ($RPV = 1 - e^{-N}$) (ref. 42). Therefore, at each concentration, the quantification error was estimated by the number of positive voxels ($Error = 1/\sqrt{N_{positive\ voxel}}$) (ref. 43). The number of voxels to be measured was estimated to obtain a required accuracy based on the RPV determined from the calibration curve.

Pre-calibration

Not all analytes may be effectively measured with dCERS. The analytes of interest should have well-defined and specific spectral signatures that can be extracted from the background, as well as adequate interactions with hotspots to produce marked enhancement so that the signal-to-noise ratio is sufficiently robust. Moreover, as several factors can influence the detection efficiency of the analytes for dCERS, it is

difficult to formulate predictions on a theoretical basis. Therefore, a pre-requisite is to perform a series of experiments for each analyte, so that the appropriate spectral features (window choice and wavelength) with sufficient quality can be determined and the colloidal functionalization can be optimized, which will serve as the basis for subsequent measurements. A second issue to consider is the differences in detection efficiency owing to uncontrollable variations in the fabrication process of the SERS colloids, leading to differences in concentration, enhancement factor and affinity to the analytes. For each freshly made batch of colloids, a small fraction should be taken out and examined with various analytes in the appropriate concentration range. Therefore, these calibration curves are necessary for each batch to convert the measured positive counts into quantitative measurements.

Apparent efficiency

In a practical sense, it is suggested to use an index to quantitatively depict all influencing factors on the dCERS calibration curve. We have defined the dCERS apparent efficiency in the standardized detection conditions, expressed as the number of positive pixels under a certain measurement duration and concentration of the analytes and the metallic colloids (that is, 1,000 s at 10^{-10} M of analytes and 0.5 nM SERS colloids in this work). With this definition, the apparent efficiencies of all of the detection systems discussed in the paper have been listed in Extended Data Table 1. From the apparent efficiency, we are able to obtain some insights into the dCERS properties based on the molecule–colloid interaction. On the basis of apparent efficiency, the measurement parameters (for example, the total number of voxels) can also be optimized to meet the quantitative demands under the potential analyte concentration and the current measurement conditions. It is also an index to instruct the choice of appropriate SERS colloids and instrumentation settings.

Quantification by analog method

With each concentration, three independent measurements were performed with 5,400 voxels (that is, 5,400 spectra) per test. We summed all the acquired spectra in one test (n = 5,400) in the first step, followed by baseline removal and intensity reading from the signature window. After subtraction of the intensity from the null control, we obtained the mean and error from the three tests at each concentration. For a comparison between the conventional analog method and dCERS, we examined the two methods when applied to the same spectral dataset, namely, the data of crystal violet enhanced by the Hya–Ag colloids at a concentration of 10^{-10}–10^{-15} M (Extended Data Fig. 1).

Reporting summary

Further information on research design is available in the Nature Portfolio Reporting Summary linked to this article.

Data availability

Source data are provided with this paper. The other relevant data are available from the corresponding author upon request.

36. Leopold, N. & Lendl, B. A new method for fast preparation of highly surface-enhanced Raman scattering (SERS) active silver colloids at room temperature by reduction of silver nitrate with hydroxylamine hydrochloride. *J. Phys. Chem. B* **107**, 5723–5727 (2003).
37. Lee, P. C. & Meisel, D. Adsorption and surface-enhanced Raman of dyes on silver and gold sols. *J. Phys. Chem.* **86**, 3391–3395 (1982).
38. Sulaiman, S. A. J., Bora, T. & Abou-Zied, O. K. Spectroscopic characterization of the warfarin drug-binding site of folded and unfolded human serum albumin anchored on gold nanoparticles: effect of bioconjugation on the loading capacity. *RSC Adv.* **8**, 7523–7532 (2018).
39. Cohen, L. et al. Single molecule protein detection with attomolar sensitivity using droplet digital enzyme-linked immunosorbent assay. *ACS Nano* **14**, 9491–9501 (2020).
40. Ru, E. C. L., Meyer, M. & Etchegoin, P. G. Proof of single-molecule sensitivity in surface enhanced Raman scattering (SERS) by means of a two-analyte technique. *J. Phys. Chem. B* **110**, 1944–1948 (2006).
41. Wang, J. & Guo, X. Adsorption isotherm models: classification, physical meaning, application and solving method. *Chemosphere* **258**, 127279 (2020).
42. Rissin, D. M., Wilson, D. H. & Duffy, D. C. in *The Immunoassay Handbook* 4th edn (ed. Wild, D.) 223–242 (Elsevier, 2013).
43. Cherry, S. R., Sorenson, J. A. & Phelps, M. E. *Physics in Nuclear Medicine* (Elsevier Health Sciences, 2012).

Acknowledgements We thank H. Gu, H. Xu and F. Shen for their discussions. This work was supported by grants to J.Y. (National Natural Science Foundation of China, grant no. 82272054; Science and Technology Commission of Shanghai Municipality, grant no. 21511102100; Shanghai Key Laboratory of Gynecologic Oncology; and Shanghai Jiao Tong University, grant no. YG2024LC09), D.M.C. (National Natural Science Foundation of China, grant no. 32370572) and Z.S. (National Natural Science Foundation of China, grant no. 81627801; and National Key R&D Program of China, grant no. 2020YFA0908100). Z.S. was also supported by the K. C. Wong Education Foundation (Hong Kong).

Author contributions J.Y. and X.B. conceived and designed the project. X.B. performed all the experiments. Z.S. made conceptual contributions to data analysis and interpretation and supervised the revision efforts. D.M.C. contributed to mechanistic interpretations. J.Y. and Z.S. are the senior authors of this study, and all authors participated in data analysis and paper preparation.

Competing interests The authors declare no competing interests.

Additional information
Supplementary information The online version contains supplementary material available at https://doi.org/10.1038/s41586-024-07218-1.

Correspondence and requests for materials should be addressed to Jian Ye.

Peer review information *Nature* thanks Peter Vikesland and the other, anonymous, reviewer(s) for their contribution to the peer review of this work. Peer reviewer reports are available.

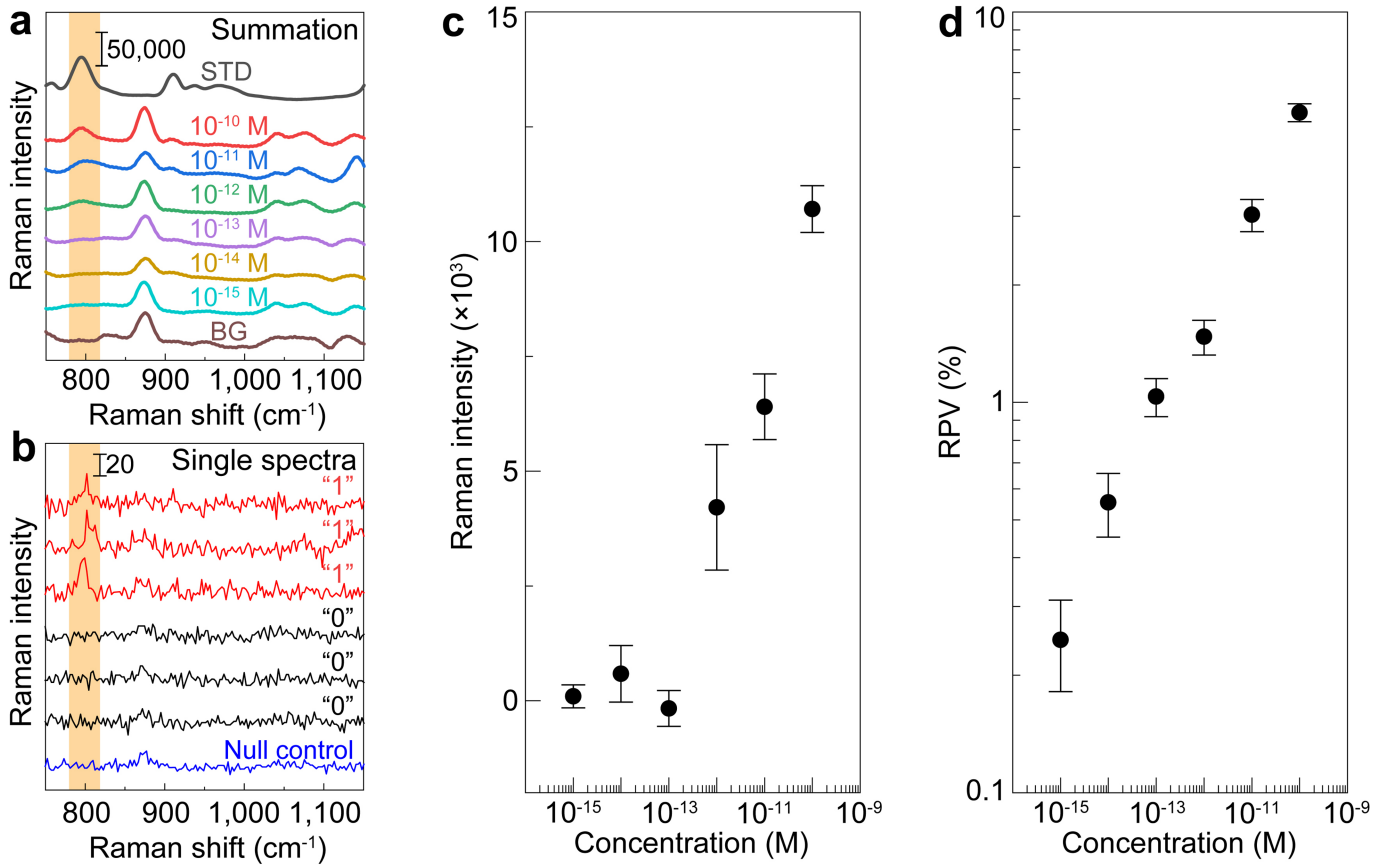

Extended Data Fig. 1 | Comparison between the analog method and dCERS. Crystal violet (CV) was quantified in the concentration range of 10^{-10} to 10^{-15} M. (a) The summation of all acquired spectra at different concentrations of CV (10^{-15} to 10^{-10} M) and background (BG) reference (null control). The standard (STD) SERS spectra of the CV-ethanol solution is provided after scaling for clarity. In the CV-specific window of 780 to 820 cm^{-1}, a weak peak was observable at concentrations from 10^{-10} to 10^{-12} M, but no peak was evident at concentrations lower than 10^{-13} M, similar to what is observed with the null control under the same conditions. (b) Typical single-molecule spectra acquired from the voxels at 10^{-15} M CV. Red: positive spectra with discernable CV-specific peaks (1); black: negative spectra without the targeted signals (0); blue: spectrum acquired in without CV (null control). The specific SERS band corresponding to CV (780 to 820 cm^{-1}) is indicated by the orange stripes in panels a and b. (c) The peak intensity from the summed spectra over all voxels versus CV concentration. The standard deviation increases rapidly as the concentration decreases and no concentration below 10^{-12} M could be reliably measured. (d) The ratio of positive voxels (RPV) versus CV concentration. The RPV decreases as the concentration decreases with the standard deviation (error bar) following Poisson statistics, and at concentrations of 10^{-11} and 10^{-12} M, the accuracy is also better than the summed case. Furthermore, as there is no evidence of a plateau region at the lowest concentrations, it is likely that much lower concentrations could be measured by the digital approach, which would clearly not be possible with the analog method. Here for panels c and d, each data point reflects the mean and the standard deviations calculated from 3 independent measurements (5,400 voxels/mapping).

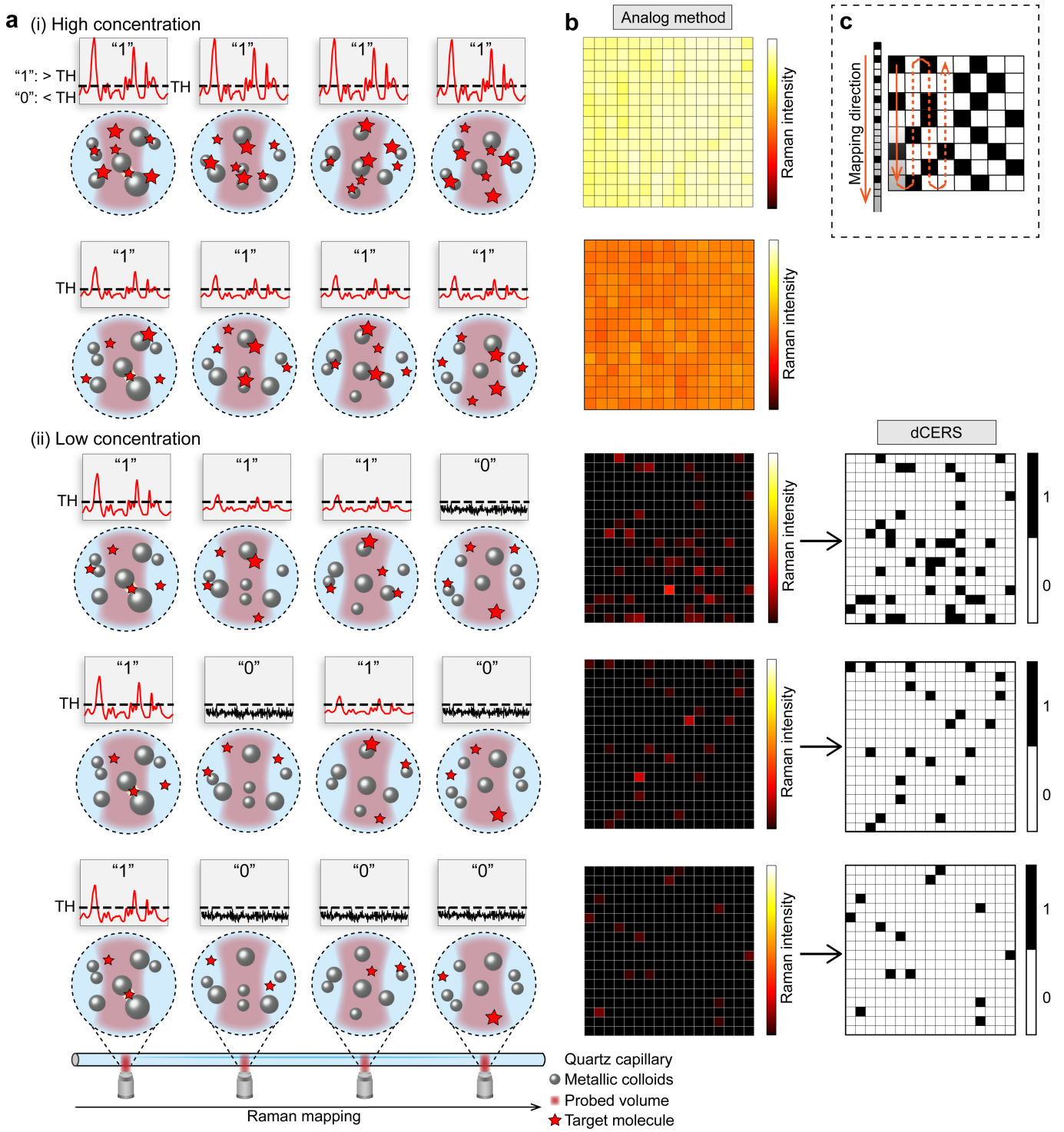

Extended Data Fig. 2 | Quantitative SERS. (a) Schematic diagrams of quantification at different concentrations. (i) High-concentration scenarios: there are multiple molecules in each excitation volume, generating recognized SERS signals with intensities higher than the threshold (TH) (positive, defined as "1") for the majority of voxels. (ii) Low-concentration scenarios: Some of the voxels show no recognizable signals, i.e., the targeted peak presents intensity that is lower than threshold (negative, defined as "0"). (b) Heatmaps demonstrate the ability to quantify the magnitude of the target intensities in scenario (i) yet failure in scenario (ii) because of severe SIFs. By contrast, the ratio of positive voxels per mapping, reflected by digital maps (indicated by rightwards arrows) obtained by dCERS, still possess clear correlation with the concentrations in scenario (ii). (c) Schematic diagram of the depictions of the digital/heat maps. The stripe-like mapping areas are rearranged into squares for this presentation.

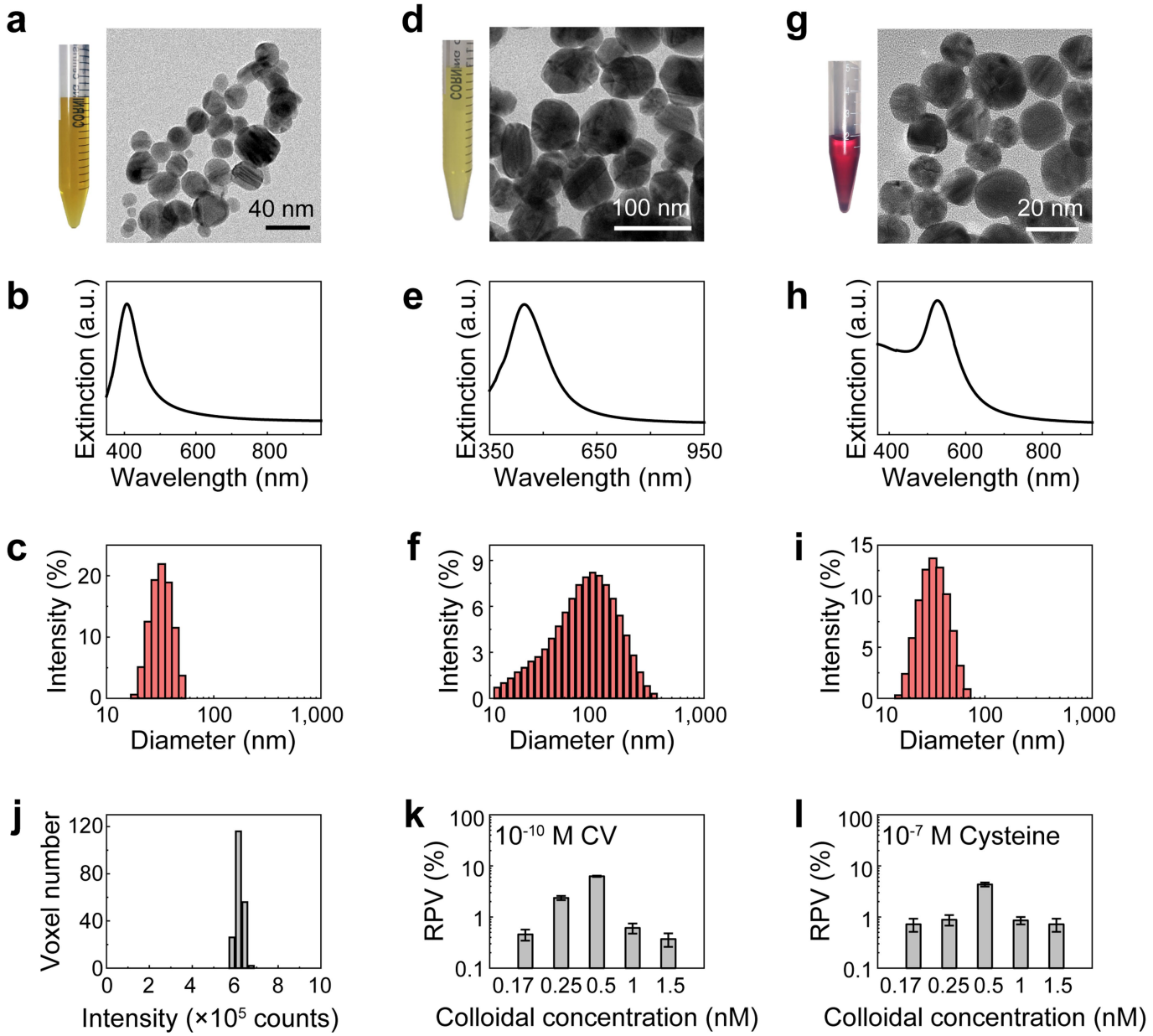

Extended Data Fig. 3 | Characterization of the SERS colloids. (a)-(c) Hya-Ag colloids, (d)-(f) citrate-Ag colloids and (g)-(i) citrate-Au colloids. (a), (d), (g) Shown are the colloidal suspensions contained in the vials (left) and transmission electron microscopic images of the colloids (right). (b), (e), (h) Extinction spectra. (c), (f), (i) Histograms of the hydrodynamic diameter obtained by dynamic light scattering. (j) Histogram of the intensity distribution among voxels in 10^{-7} M crystal violet detected by Hya-Ag colloids. The relative standard deviation is 2.8% among the 200 voxels, indicating that the hotspots present in each probed voxel were statistically comparable across voxels. To improve statistics, a relatively longer acquisition time was used for each voxel (i.e., 5 s) to accumulate more hotspots. (k) 10^{-10} M crystal violet (CV) and (l) 10^{-7} M L-cysteine were detected by the Hya-Ag colloids at 0.17, 0.25, 0.5, 1 and 1.5 nM. The detection efficiency is improved when the colloidal concentration increases, because of the increased hotspot density. With greater colloid concentration, the detection efficiency then decreases due to the increased background scattering. The histograms show the RPVs with error bars indicating the standard deviations (n = 3). The optimal concentration for Hya-Ag colloids was found around 0.5 nM.

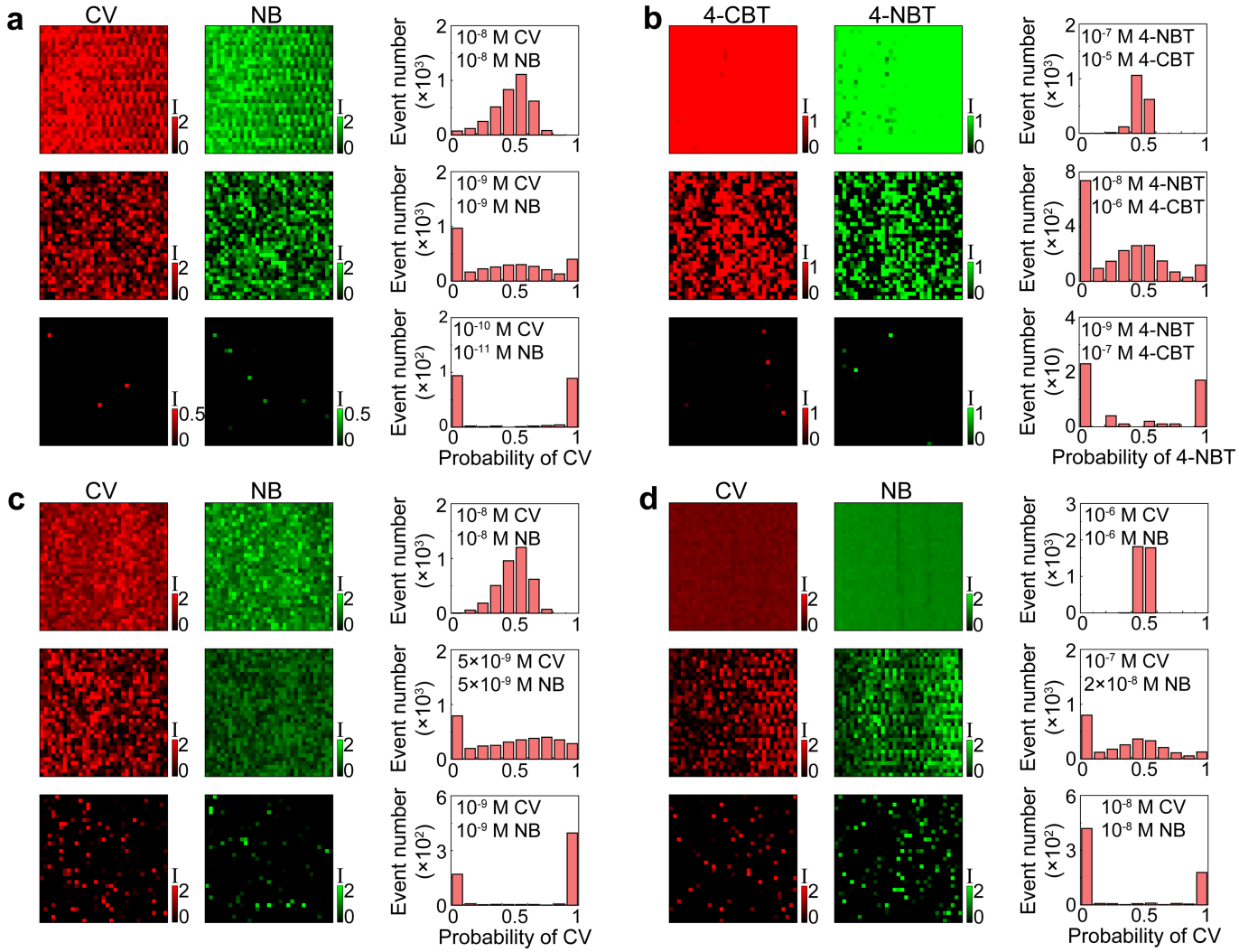

Extended Data Fig. 4 | Single-molecule sensitivity by BiASERS. The concentration-dependent heatmaps of each analyte involved in the BiASERS measurements (left and middle) and the histograms of the contribution of (a, c, d) crystal violet (CV) or (b) 4-NBT in each spectrum (right). The pure events are defined as the probability of one of the analytes approaching 0 (or 1) and the mixed events are defined as the probability in between. (a) Mixtures of CV and Nile blue (NB) measured using Hya-Ag colloids. At 10^{-8} M of CV/NB, both analytes show clear signal in nearly all voxels, exhibiting a Gaussian-like histogram of the probability of CV. On the contrary, at 10^{-9} M CV, some spectra exhibit neither the CV nor NB signal but within all signal spectra, there is a growing proportion of pure-signaled ones, leading to an increase of 1/0 measurements than those in the middle. At 10^{-10} M CV, most signal spectra exhibit pure signals with extremely rare ones showing both signals. Since these pure-signaled spectra should be statistically dominated by single-molecule events, the single-molecule regime for CV should be below 10^{-9} M. (b) Mixture of 4-NBT and 4-chlorothiophenol (4-CBT) measured using Hya-Ag colloids, exhibiting the expected single-molecule behavior for 4-NBT below 10^{-8} M. (c) Mixtures of CV and NB measured by citrate-Ag colloids and (d) citrate-Au colloids. The same trend can be observed in the other types of SERS colloids though at different analyte concentrations due to differences in hotspot density/intensity, surface binding affinity, among other properties.

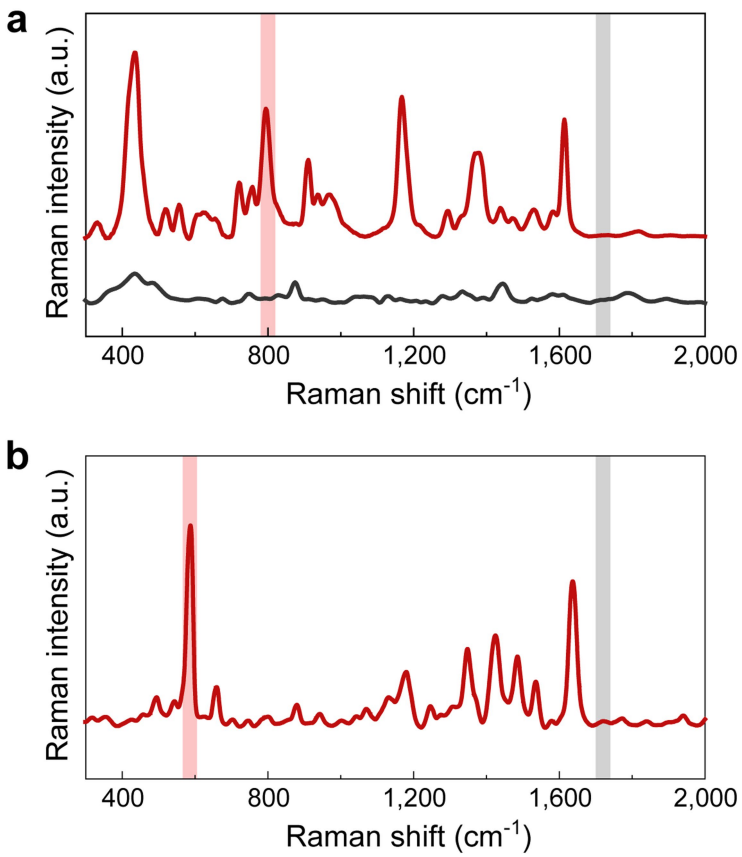

Extended Data Fig. 5 | Standard SERS spectra. (a) The standard SERS spectrum of 10^{-7} M crystal violet enhanced by Hya-Ag colloids (red) and the averaged spectrum of the null control (black). The signature window of crystal violet at 780 to 820 cm^{-1} is indicated by the red stripe. (b) The standard SERS spectrum of 10^{-7} M Nile blue enhanced by Hya-Ag colloids. The signature window of Nile blue at 565 to 605 cm^{-1} is indicated by the red stripe. For both panels, the noise window is at 1,700 to 1,740 cm^{-1} as indicated by the gray stripes.

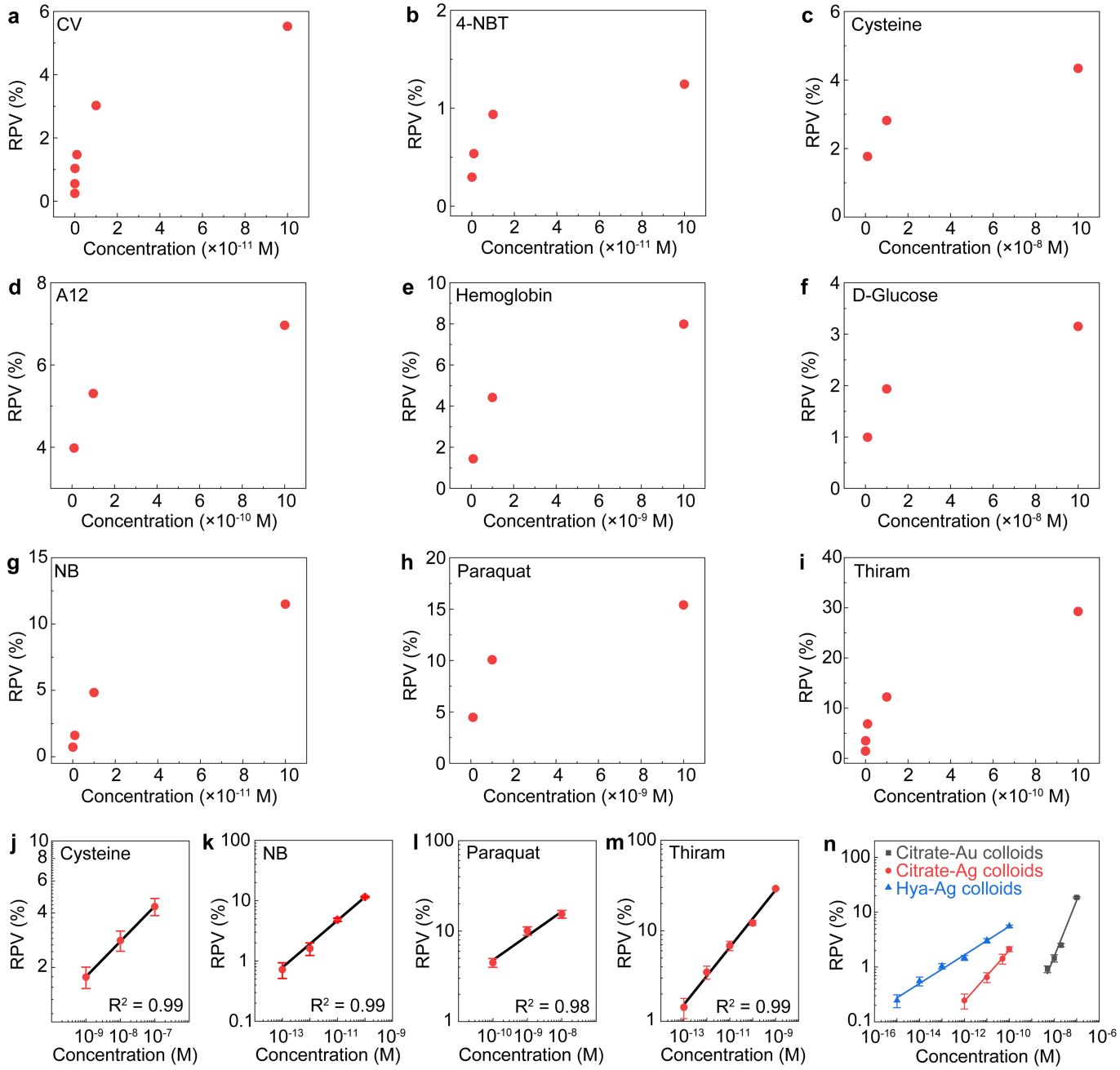

Extended Data Fig. 6 | dCERS of different analytes and using different colloids. The relationship between RPV and analyte concentrations of (a) crystal violet (CV), (b) 4-NBT, (c) cysteine, (d) A12, (e) hemoglobin, (f) D-glucose, (g) Nile blue (NB), (h) paraquat and (i) thiram measured using Hya-Ag colloids plotted in a linear-linear scale. The calibration curves of (j) cysteine, (k) NB, (l) paraquat and (m) thiram measured using Hya-Ag colloids. The cysteine shows a much lower efficiency than 4-NBT likely owing to a smaller molecular cross section assuming that both have a high affinity to Hya-Ag colloids via covalent binding. (n) The calibration curves of CV using Hya-Ag colloids (blue), citrate-Ag colloids (red) and citrate-Au colloids (black). Though the three different types of colloids have comparable surface potential and concentration, citrate-Au colloids exhibit a much lower efficiency than the other two Ag colloids due to a poorer plasmonic effect. Additionally, the efficiency of citrate-Ag colloids is slightly lower than Hya-Ag colloids probably because of a layer of citrate residues which may cause steric hindrance to impede CV from getting close to the metallic surface to some extent even though the size of citrate-Ag colloids is larger than Hya-Ag colloids. For the calibration curves, the error bars indicate the standard deviations calculated with 3 independent measurements. Fitting formula: $\log RPV = k \log M + b$.

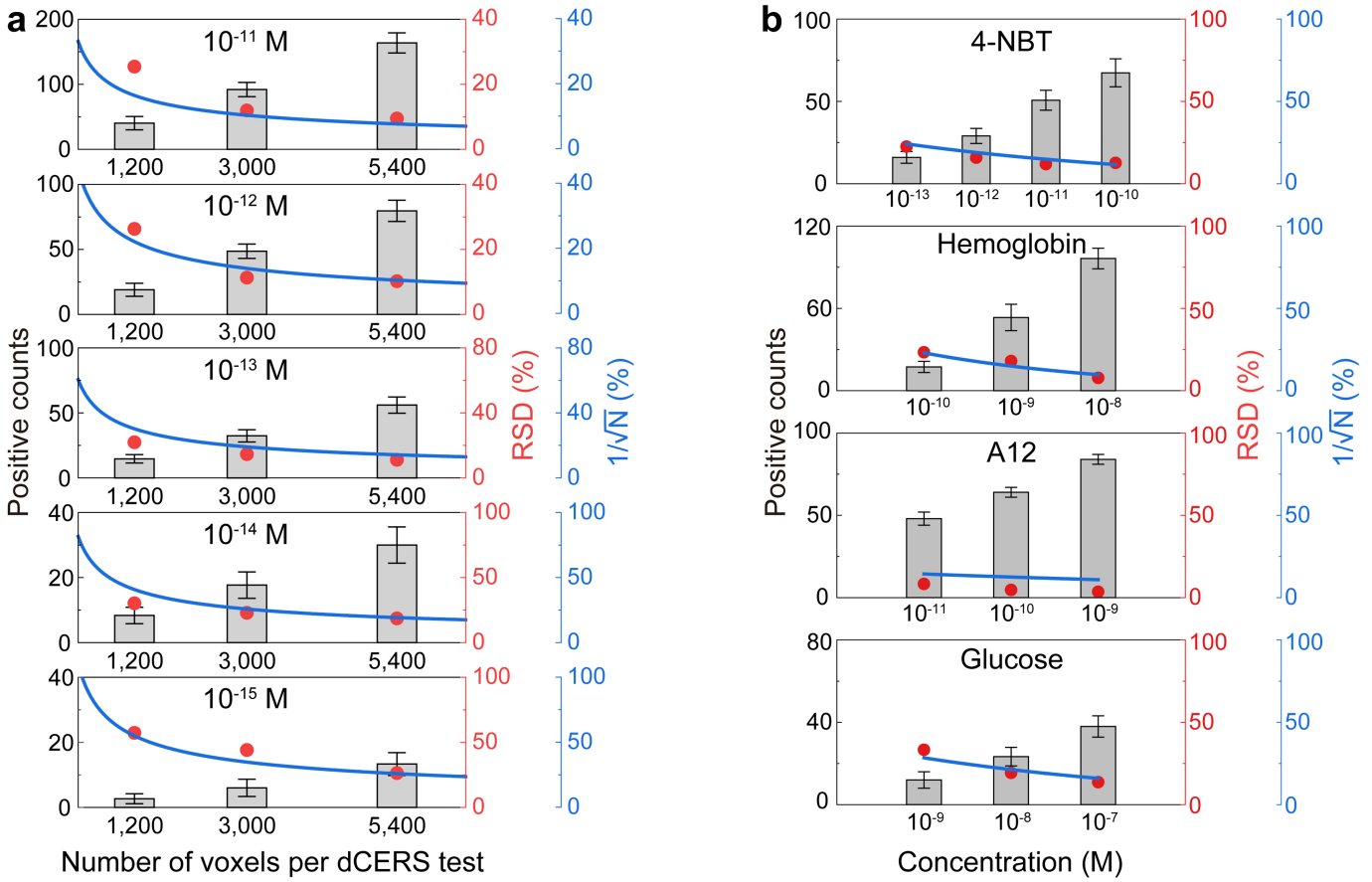

Extended Data Fig. 7 | Verification of Poisson dominated accuracy for dCERS. (a) The number of positive voxels increases with an increase in the total number of voxels acquired per dCERS test for crystal violet concentrations of 10^{-11} to 10^{-15} M crystal violet (from top to bottom) measured using Hya-Ag colloids. (b) The number of positive voxels increased with an increase in the concentration of 4-NBT, hemoglobin, A12 and glucose (from top to bottom) measured using Hya-Ag colloids. The total number of measured voxels per dCERS test was 5,400 for 4-NBT and 1,200 for the others. The gray bars show the mean number of positive voxels with the error bars indicating the standard deviations from 3 independent tests. The relative standard deviation (RSD, red dots) is calculated as the ratio of the standard deviation to the mean of the positive count, which agrees with the Poisson estimation ($\frac{1}{\sqrt{N}}$, blue lines) from the mean positive counts (N).

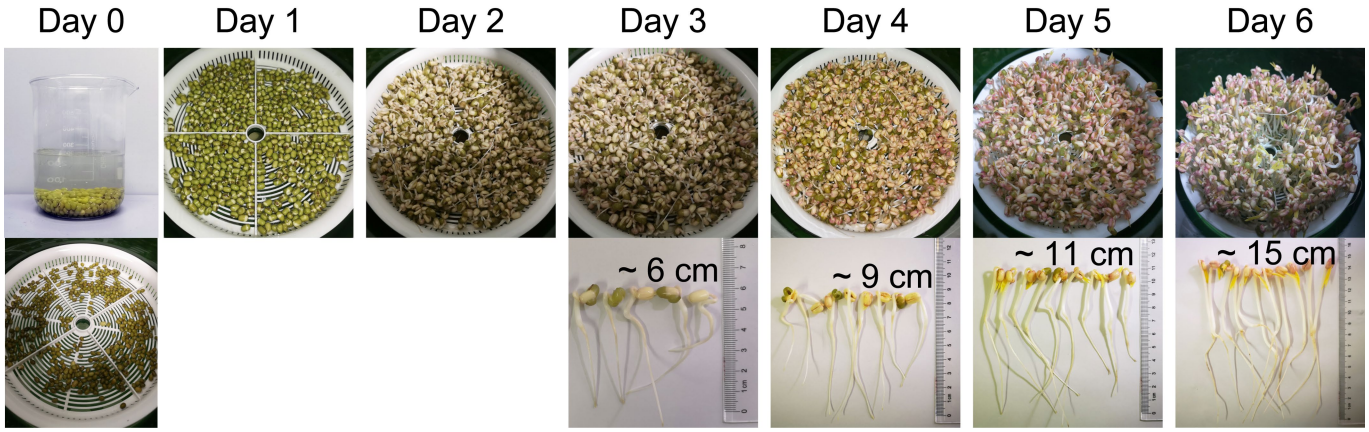

Extended Data Fig. 8 | Photographs of the lab-grown bean sprouts prepared under normal culture conditions. In brief, 50 g mung beans were immersed in pure water for 2 h and then placed in the bean sprouter with 1 L fresh pure water without thiram. From Day 1 to Day 2, the beans doubled in size and started to sprout. On each of the following days, the length of several bean sprouts was measured by a ruler.

Extended Data Table 1 | Apparent efficiency of dCERS measurements of different target molecules enhanced by different colloids

Normalized apparent efficiency (Positive voxels / 1,000 sec at 10^{-10} M target molecules and 0.5 nM SERS colloids)						
SERS colloids	Laser: 638 nm Acquisition time: 0.1 sec		Laser: 638 nm Acquisition time: 1 sec		Laser: 532 nm Acquisition time: 1 sec	
Hya-Ag	CV	552	A12	52.9	Glucose	5.77
			L-cysteine	11.4		
			Hemoglobin	15.7		
	4-NBT	136	Paraquat	47.7		
			Thiram	131.36		
Citrate-Ag	CV	202	/		/	
Citrate-Au	CV	1.41	/		/	

Extended Data Table 2 | Parameters used for the positive determination of different target molecule

Measurement parameters	Target molecule	Signature window (cm^{-1})	Noise window (cm^{-1})	Threshold
Laser: 638 nm	CV	780-820	1,700-1,740	$\bar{x} + 10\sigma$
Power: 12.67 mW	NB	565-605	1,700-1,740	$\bar{x} + 10\sigma$
Acq. time: 0.1 sec	4-NBT	1,305-1,345	1,700-1,740	$\bar{x} + 10\sigma$
	Hemoglobin	655-695	1,700-1,740	$\bar{x} + 5\sigma$
Laser: 638 nm	Cysteine	635-675	1,700-1,740	$\bar{x} + 5\sigma$
Power: 12.67 mW	A12	710-760	1,950-2,000	$\bar{x} + 5\sigma$
Acq. time: 1 sec	Thiram	1,360-1,400	1,700-1,740	$\bar{x} + 5\sigma$
	Paraquat	1,620-1,660	1,700-1,740	$\bar{x} + 5\sigma$
Laser: 532 nm				
Power: 37.3 mW	Glucose	1,120-1,160	1,760-1,800	$\bar{x} + 10\sigma$
Acq. time: 1 sec				

nature portfolio

Corresponding author(s): Jian Ye

Last updated by author(s): Jan 28, 2024

Reporting Summary

Nature Portfolio wishes to improve the reproducibility of the work that we publish. This form provides structure for consistency and transparency in reporting. For further information on Nature Portfolio policies, see our Editorial Policies and the Editorial Policy Checklist.

Statistics

For all statistical analyses, confirm that the following items are present in the figure legend, table legend, main text, or Methods section.

n/a	Confirmed	
☐	☒	The exact sample size (*n*) for each experimental group/condition, given as a discrete number and unit of measurement
☐	☒	A statement on whether measurements were taken from distinct samples or whether the same sample was measured repeatedly
☒	☐	The statistical test(s) used AND whether they are one- or two-sided *Only common tests should be described solely by name; describe more complex techniques in the Methods section.*
☒	☐	A description of all covariates tested
☒	☐	A description of any assumptions or corrections, such as tests of normality and adjustment for multiple comparisons
☐	☒	A full description of the statistical parameters including central tendency (e.g. means) or other basic estimates (e.g. regression coefficient) AND variation (e.g. standard deviation) or associated estimates of uncertainty (e.g. confidence intervals)
☒	☐	For null hypothesis testing, the test statistic (e.g. *F*, *t*, *r*) with confidence intervals, effect sizes, degrees of freedom and *P* value noted *Give P values as exact values whenever suitable.*
☒	☐	For Bayesian analysis, information on the choice of priors and Markov chain Monte Carlo settings
☒	☐	For hierarchical and complex designs, identification of the appropriate level for tests and full reporting of outcomes
☒	☐	Estimates of effect sizes (e.g. Cohen's *d*, Pearson's *r*), indicating how they were calculated

Our web collection on statistics for biologists contains articles on many of the points above.

Software and code

Policy information about availability of computer code

Data collection	LabSpec 6.5 was used to collect the Raman spectra.
Data analysis	MATLAB R2020b was used for spectral analysis.

For manuscripts utilizing custom algorithms or software that are central to the research but not yet described in published literature, software must be made available to editors and reviewers. We strongly encourage code deposition in a community repository (e.g. GitHub). See the Nature Portfolio guidelines for submitting code & software for further information.

Data

Policy information about availability of data

All manuscripts must include a data availability statement. This statement should provide the following information, where applicable:

- Accession codes, unique identifiers, or web links for publicly available datasets
- A description of any restrictions on data availability
- For clinical datasets or third party data, please ensure that the statement adheres to our policy

Source data for Figures 1-3, Extended Data Figures 1-9 and Extended Data Table are provided with the paper. The other relevant data are available from the corresponding author upon request.

Human research participants

Policy information about studies involving human research participants and Sex and Gender in Research.

Reporting on sex and gender	No human researches were performed, so there is no reporting on sex and gender in this manuscript.
Population characteristics	No information about population characteristics is provided since this manuscript doesn't include human research participants.
Recruitment	Information about recruitment is not provided since this manuscript doesn't include human research participants.
Ethics oversight	No ethics oversight is provided since this manuscript doesn't include human research participants.

Note that full information on the approval of the study protocol must also be provided in the manuscript.

Field-specific reporting

Please select the one below that is the best fit for your research. If you are not sure, read the appropriate sections before making your selection.

☒ Life sciences ☐ Behavioural & social sciences ☐ Ecological, evolutionary & environmental sciences

For a reference copy of the document with all sections, see nature.com/documents/nr-reporting-summary-flat.pdf

Life sciences study design

All studies must disclose on these points even when the disclosure is negative.

Sample size	No statistical methods were used to pre-determine the sample size. Experiments were done in triplicate.
Data exclusions	No sample was excluded from data analysis.
Replication	The results were successfully replicated.
Randomization	The samples were measured randomly for the detection of different concentrations of analytes.
Blinding	No blinding was employed since all experiments are in vitro.

Reporting for specific materials, systems and methods

We require information from authors about some types of materials, experimental systems and methods used in many studies. Here, indicate whether each material, system or method listed is relevant to your study. If you are not sure if a list item applies to your research, read the appropriate section before selecting a response.

Materials & experimental systems

n/a	Involved in the study
☒	☐ Antibodies
☒	☐ Eukaryotic cell lines
☒	☐ Palaeontology and archaeology
☒	☐ Animals and other organisms
☒	☐ Clinical data
☒	☐ Dual use research of concern

Methods

n/a	Involved in the study
☒	☐ ChIP-seq
☒	☐ Flow cytometry
☒	☐ MRI-based neuroimaging